2017

Wearable Passive Wireless MEMS Respiration Sensor

Sina Moradian
University of Central Florida

WEARABLE PASSIVE WIRELESS MEMS RESPIRATION SENSOR

by

SINA MORADIAN
B.S. Iran University of Science and Technology, 2013

A thesis submitted in partial fulfilment of the requirements
for the degree of Master of Science
in the Department of Electical and Computer Engineering
in the College of Engineering and Computer Science
at the University of Central Florida
Orlando, Florida

Spring Term
2017

ABSTRACT

In this study a passive sensor that wirelessly monitors the profile of the human respiratory system is presented. The sensor was designed to be wearable, weighs less than 10 grams and is durable. The sensor is made of a RF piezoelectric MEMS resonator and an ultra-high frequency antenna made of a thin metal film formed on a flexible substrate . The resonance frequency of the TPoS resonator shifts as a function of condensation and evaporation of water vapor on the surface of the resonator and changes in resonator's temperature. These parameters change in each in response to inspiration and expiration and a wireless measurement system detects the frequency shift of the sensor and converts it into the respiration profile. The respiration profile of a healthy human subject is measured and presented for a transmitter to sensor to receiver distance of 25cm.

ACKNOWLEDGMENTS

I would like to thank my family, advisor, and colleagues for their support.

TABLE OF CONTENTS

LIST OF FIGURES

LIST OF TABLES

CHAPTER 1: INTRODUCTION

Respiration, the movement of air into and out of the lungs, contains significant amounts of information on status of human health. Along with blood pressure, temperature, and pulse rate, respiration rate is one of the four vital signs [6] essential for monitoring by medical professionals. Monitoring the respiration rate has led been proven to be correlated to conditions such as cardiac arrest and metabolic acidosis [7]. Furthermore, it has been shown to be a better indicator than blood pressure or pulse rate for identifying at-risk patients for admission to intensive care units [8].

Respiration rate sensors can be divided into contact and noncontact methods [9]. In noncontact methods the movement of the chest region is monitored by a thermal, optical, or radar imaging system [9]. Noncontact methods have the advantage of not requiring the attachment of any restrictive equipment to the patient, however, they are susceptible to disruption of operation from the movement of the patient. In contact methods parameters such as respiration temperature, respiratory sounds, respiration flow, chest movement, and respiratory CO_2 emission are monitored. Currently the gold standard for monitoring the respiration system is the measurement of air flow using a temperature sensor [10]. In this method, a temperature sensor such as a thermistor or thermocouple is placed in the nasal or oral track to measure air flow temperature.

To measure any of the above parameters using contact methods the patient is connected to a relatively bulky sensing unit with tubes and/or electrical wires depending on the measurement system. In addition to being highly uncomfortable, the size of such devices immobilizes the patient, thus rendering continuous monitoring impossible.

To address these issues a wireless sensor is created in this work. Ideally a wireless sensor should be small, lightweight, flexible, inexpensive, and durable. For the realization of these goals we have opted for a passive wireless system instead of incorporating a battery in the sensor. Our

passive wireless sensor is composed of an antenna and a MEMS resonator, with the latter being responsible for the detection of the respiration profile. In addition to being highly sensitive to changes in respiration flow to operate passively the resonator needs to have low loss and a high quality factor.

CHAPTER 2: PIEZOELECTRIC MEMS RESONATORS

Piezoelectric Material

Charge distribution in atoms has a significant effect on their ability to form bond(s) with other atoms and the types of bonds they form. The distribution of positive and negative charges of an atom, and more generally molecules, can be simplified as an electric dipole composed of a positive and negative point charge. The moment of a dipole is a function the charge of individual atoms and the geometry of the molecule. As an example the charge distribution of a water molecule is shown in Fig. 2.1 . Since oxygen has a higher electronegativity, hydrogens' electrons spend more time closer to the oxygen atom than hydrogen atoms. As a result oxygen has a net negative charge and hydrogen has a net positive charge. Because the center of positive and negative charges are not the same this molecule can be simplified as an electric dipole.

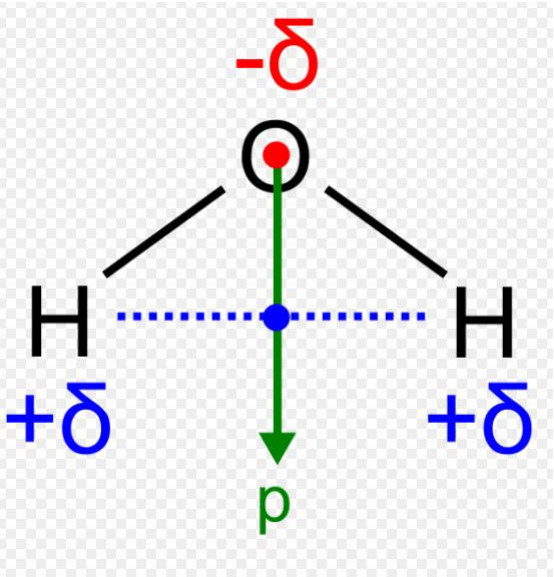

Figure 2.1: Charge distribution in a water molecule [1]

When a molecule is placed in an electric field the positive and negative charges are pushed in opposite directions. For many molecules this results in a change in the geometry of the molecule. In the case of a H_2O molecule if the electric field is applied parallel to the dipole the two hydrogen atoms are pushed in the opposite direction compared to the oxygen atom. This increases the dipole moment. In piezoelectric material an electrical field increases the dipole moment, however unlike non-pizoelectric material, the displacement caused by this increase is not symmetric, meaning that the dipole experiences a net displacement. Rather than a single molecule, it's most useful when a number of molecules are aligned in the same direction and form a crystal. Up to this point an intuitive understanding of the relation between charge distribution and displacement caused by an external electric field has been established. In the following section we seek to quantify this relationship.

The polarization vector defined by Eq.2.1 is the average electric dipole moment as a function of

the electric field E and electric displacement field D.

$$P = D - eE \tag{2.1}$$

Here e is the charge of an electron. If the material under study is nonhomogeneous or anisotropic P, D, and E are matrices. In thie case of homogeneous and isotropic material $P = P_0 I$, where I is the unit matrix and P_0 is the scalar value of the polarization vector.

Alternatively the polarization density can be defined as Eq.2.2.

$$P = \frac{\Delta P}{\Delta V} \tag{2.2}$$

where ΔP is the dipole moment contained in volume of ΔV.

The stress-strain relationship for linear material according to Hook's law is given by Eq.2.3.

$$S = sT \tag{2.3}$$

Where S is the strain tensor, T is the stress tensor, and s is the compliance matrix.

This equation does not apply to piezoelectric material as it fails to take into account the effect of electric dipoles on the stress and strain of a material.

When placed in an electric field the moment of an electric dipole increases. This increase exhibits itself in the amount of positive and negative charge and also the distance between the two charges. These two effects are also correlated as the amount of charge results in an increase in the Coulomb force between the positive and negative charges. The displacement of the positive and negative

charges results in force being applied to adjacent dipoles.

Mechanical strain is defined as Eq.2.4.

$$S = \frac{\Delta L}{L_0} \tag{2.4}$$

In this equation L_0 is the initial length and ΔL is the change in length. In piezoelectric material the change in length caused by an electric field has a linear relation with the electric field. Using the superposition principle the total strain in a piezoelectric material is calculated using Eq.2.5.

$$S = sT - d_t E \tag{2.5}$$

Where s is the compliance and d_t is the transpose of the piezoelectric coefficient.

The generation of an electric field as a result of an applied stress or force is called the reverse piezoelectric effect. To quantify this relation we rely on the polarization vector. Assuming that the polarization has a direct relation with stress we can define polarization as Eq.2.6.

$$P = dT \tag{2.6}$$

If Eq.2.6 is placed in Eq.2.1 we can calculate the reverse piezoelectric effect as Eq.2.7 .

$$D = \varepsilon E + dT \tag{2.7}$$

Where ε is the permittivity of the piezoelectric material. Eq.2.7 with Eq.2.5 are coupled together and are typically both required for calculating the properties of piezoelectric MEMS devices. Stress

has 3 independent longitudinal and 6 independent shear components [11]. This means that the stress matrix, T is a 9×9 matrix. Using assumptions of continuum mechanics it can be shown that stress can be defined using only a 6×6 matrix [11]. Similarly the strain matrix can be reduced to a 6×1 matrix. The top 3 elements represent the normal components of stress and strain, x, y and z respectively, and the 6 lower elements represent the shear components. The compliance and piezoelectric matrices can also be simplified according to the symmetries of the crystal structure. For AlN, the piezoelectric material used in this work, Eq.2.5 can be rewritten as Eq.2.8.

$$\begin{bmatrix} S_1 \\ S_2 \\ S_3 \\ S_4 \\ S_5 \\ S_6 \end{bmatrix} = \begin{bmatrix} s_{11}^E & s_{12}^E & s_{13}^E & 0 & 0 & 0 \\ s_{21}^E & s_{22}^E & s_{23}^E & 0 & 0 & 0 \\ s_{31}^E & s_{32}^E & s_{33}^E & 0 & 0 & 0 \\ 0 & 0 & 0 & s_{44}^E & 0 & 0 \\ 0 & 0 & 0 & 0 & s_{55}^E & 0 \\ 0 & 0 & 0 & 0 & 0 & s_{66}^E \end{bmatrix} \begin{bmatrix} T_1 \\ T_2 \\ T_3 \\ T_4 \\ T_5 \\ T_6 \end{bmatrix} + \begin{bmatrix} 0 & 0 & d_{31} \\ 0 & 0 & d_{32} \\ 0 & 0 & d_{33} \\ 0 & d_{24} & 0 \\ d_{15} & 0 & 0 \\ 0 & 0 & 0 \end{bmatrix} \begin{bmatrix} E_1 \\ E_2 \\ E_3 \end{bmatrix} \tag{2.8}$$

Similarly for this piezoelectric material the matrix form of Eq.2.7 can be written as Eq.2.9.

$$\begin{bmatrix} D_1 \\ D_2 \\ D_3 \end{bmatrix} = \begin{bmatrix} 0 & 0 & 0 & 0 & d_{15} & 0 \\ 0 & 0 & 0 & d_{24} & 0 & 0 \\ d_{31} & d_{32} & d_{33} & 0 & 0 & 0 \end{bmatrix} \begin{bmatrix} T_1 \\ T_2 \\ T_3 \\ T_4 \\ T_5 \\ T_6 \end{bmatrix} + \begin{bmatrix} \varepsilon_{11} & 0 & 0 \\ 0 & \varepsilon_{22} & 0 \\ 0 & 0 & \varepsilon_{33} \end{bmatrix} \begin{bmatrix} E_1 \\ E_2 \\ E_3 \end{bmatrix} \tag{2.9}$$

Typically engineers utilize the piezoelectric coefficient matrix, d to determine the feasibility of a specific piezoelectric material for a particular application. A second parameter used as a figure of

merit for piezoelectric material is the coupling coefficient. The coupling coefficient as formulated by Eq.2.10 is a measure of the efficiency of the conversion of mechanical energy into electrical energy and vice versa [5].

$$K = \sqrt{\frac{W_E}{W_M}} \tag{2.10}$$

Here K is the coupling coefficient W_M is the mechanical energy applied to a piezoelectric material and W_E is the stored electrical energy in the piezoelectric material. A second definition of the coupling coefficient is based on the piezoelectric coefficient matrix and summarized as Eq.2.11 [5].

$$k_{ij}^2 = \frac{d_{ij}^2}{c_{ij}^E \varepsilon_{ij}^T} \tag{2.11}$$

Here ε_{ij}^T is the dielectric constant in the ij direction for zero stress, c_{ij}^E is the stiffness coefficient in the ij direction under short circuit conditions. Below are the coupling coefficients for some common piezoelectric material.

Table 2.1: Coupling factor of common piezoelectric material [5]

Piezoelectric Material	Coupling factor ($K^2\%$)
AlN	6.5
PZT	23
Lithium Niobate	23
Quartz	0.86

In addition to the piezoelectric matrix, and the coupling factor other parameters that are taken

into account when assessing a piezoelectric material include material loss, stiffness coefficient and fabrication compatibility.

It should be noted that the parameters listed above are all subject to change with frequency. Piezoelectric materials exhibiting high piezoelectric coefficients at high frequencies may not necessary have the same properties at low frequencies.

Loss Mechanisms in Piezoelectric Material

Only a portion of a mechanical force applied to a piezoelectric material is converted to electrical energy in the piezoelectric material the remaining portion is eventually converted to heat. Generally the loss mechanisms associated with piezoelectric material can be categorized into dielectric loss, electromechanical loss, and elastic loss.

An alternating electric field applied to a dielectric field periodically displaces the positive and negative charges of electric dipoles from their center of charge . A portion if the energy stored in the electric dipoles is converted to heat in each cycle through a process known as electric relaxation [12]. The complex permittivity is formulated by Eq.2.12.

$$\varepsilon = \varepsilon' - j\varepsilon'' \tag{2.12}$$

Here, ε' and ε'' are the real and imaginary parts of the dielectric coefficient, ε. Dielectric loss is represented by ε''.

Mechanical energy stored in the form of stress and strain converts into heat through phonon-phonon and phonon-electron scattering [5]. The above loss mechanisms do not completely match the observed experimental loss in piezoelectric material, therefore an additional loss term, labeled as

piezoelectric loss, is taken into account as an imaginary component in the piezoelectric matrix. The source of this loss is not well understood and there is no consensus whether it's an independent loss mechanism or part of elastic or dielectric loss [5].

Mechanical Vibrational Modes

The reflection of acoustic waves from boundaries of a micro-structure results in the formation of standing waves in the microstructure. Formation of these standing waves is a function of the geometry and material composition of a micro-structure and the excitation frequency. If the dimensions of the microstructure are designed appropriately reflecting waves will create well defined standing waves. Formation of standing waves is the fundamental basis of MEMS devices.

A single micro-structure is capable of oscillating at specific frequencies or modes, each corresponding to the formation of a standing wave. The same microstructure operating at different modes has a different effective stiffness at each mode. Modes of vibration can be calculated by solving the eigenfunction equation for the microstructure. In this thesis we will theoretically and experimentally study the devices operating in lateral extensional mode.

Piezoelectric MEMS Devices

The reversible conversion of mechanical energy (kinetic and potential) into electrostatic energy (stored in the electric field) is used to actuate piezoelectric MEMS devices. An electric field applied to a piezoelectric layer results in the propagation of stress waves throughout the microstructure. Microstructures are designed to harness the stress waves to actuate vibration modes. Without the formation of standing waves the amount of displacement from the stress created by electrically exciting the piezoelectric layer is extremely small and not enough to effectively excite microstruc-

tures.

Thin-film Piezoelectric on Substrate Resonators

The piezoelectric MEMS devices used in this study are designed to excite the lateral extensional mode. In this mode, as shown in Fig.2.2, the micromechanical structure oscillates in plane and acoustic waves are longitudinal. To actuate this mode in a microstructure, a layer of piezoelectric material is deposited on top of the microstructure. An electric field applied in the out of plane direction results in in plane stress in the piezoelectric layer. This stress diffuses into the substrate layer and subsequently results in the formation of a standing wave that corresponds to the lateral extensional mode.

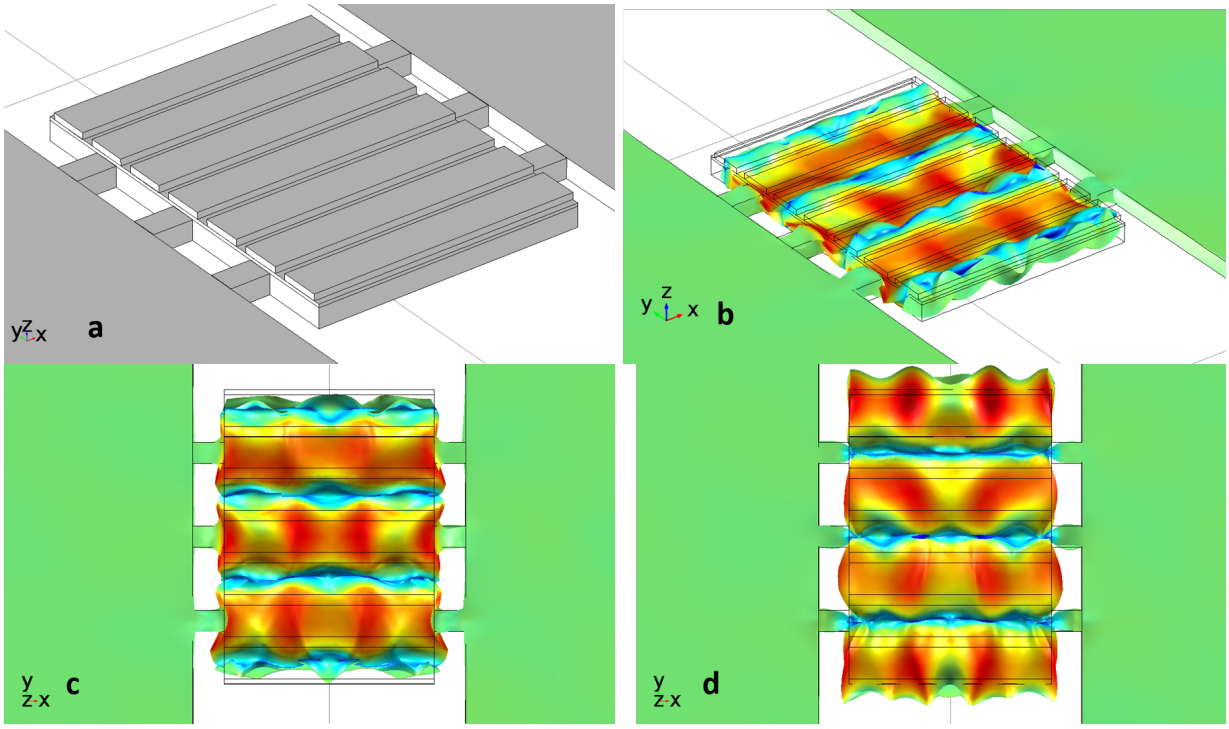

Figure 2.2: Simulation of stress in ydirection in lateral extensional mode using COMSOL multi-physics. Areas in red and blue have tensile and compressive stress, respectively. Metal electrodes are not shown to scale: (a) view of microstructure of TPOS resonator, (b) resonator excited in lateral extensional mode (displacement not shown to scale), (c) top view of TPOS resonator at maximum contraction (d) top view of at maximum extension

The structure of a TPOS device as depicted in Fig.2.3 is comprised of a thin film piezoelectric film sandwiched between two metallic electrodes all of which is in turn stacked on a substrate layer. The fundemntal concept of TPoS devices is the improvement of storage of mechanical energy in the microstructure by choosing a substrate layer with low acoustic loss. The microstructure is actuated by applying an electric field between the top and bottom electrodes. The top electrodes makeup the the input and output and the bottom electrode acts as the ground.

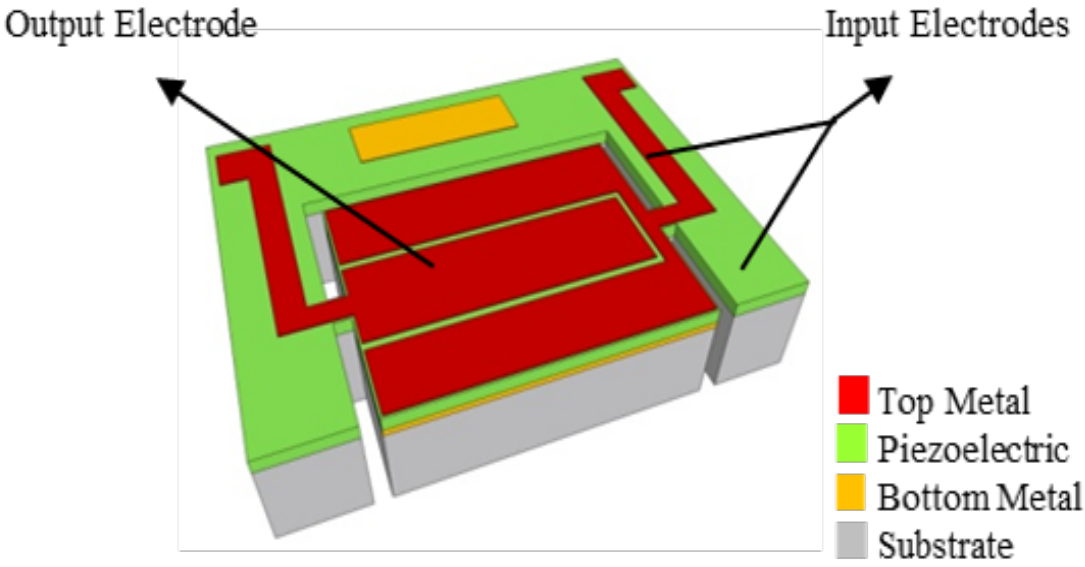

Figure 2.3: Illustration of TPoS resonator [2].

TPoS MEMS resonators have a number key advantages:

1-Increased acoustic energy storage capacity compared to piezoelectric devices but without substrate layer..

2-Acoustic waves in the substrate are subject to lower loss increased storage capacity is subject to lower material loss.

3-Increase in volume/surface results in lower surface loss.

4-Operating frequency is set by lateral dimension of microstructure enabling the fabrication of radically different designs on the same wafer.

Typically the lateral dimension of a TPoS resonator is an odd integer of the half wavelength of the longitudinal acoustic wave at resonance frequency. To calculate the wavelength the velocity needs

to be calculated first. The velocity of longitudinal acoustic waves can be calculated with Eq.2.13.

$$v = \sqrt{\frac{E}{\rho}} \tag{2.13}$$

Where v is the velocity of longitudinal acoustic wave, E is the young's modulus and ρ is the material density. Knowing the acoustic velocity While Eq.2.13 is widely utilized to calculate the velocity of longitudinal acoustic waves it should be noted that Eq.2.13 is derived using definition of stress, strain, and Newton's laws of motion for an isotropic homogeneous and uniform structure. Therefore, for our purposes Eq.2.13 only provides a rough estimate of the velocity and resonance frequency and Finite Element Methods (FEMs) are required for precise calculation of these parameters in MEMS devices.

Butterworth Van Dick Model

The BVD model derives the values of a series RLC circuit with a parallel capacitive branch according to the frequency response of the resonator. The schematic of the equivalent circuit is shown in Fig.2.4.

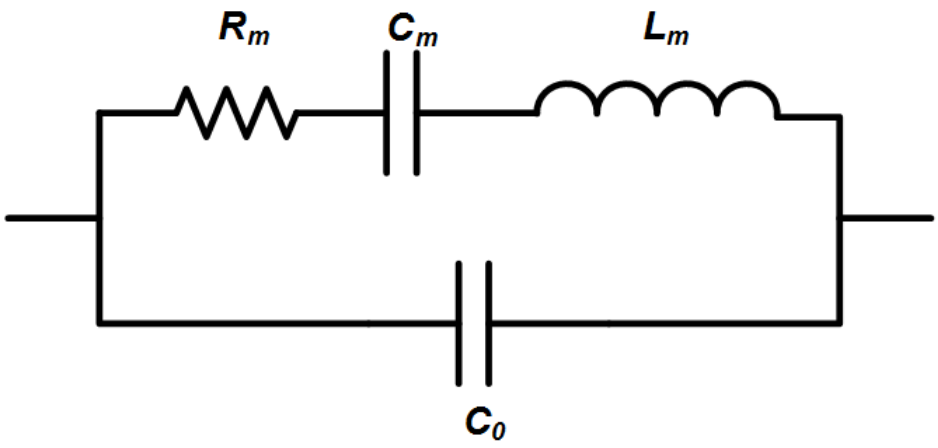

Figure 2.4: Equivalent circuit of piezoelectric MEMS resonator using BVD model [3].

The series RLC branch is the motional branch and models the mechanical oscillation of microstructure and it's effect on the electrical input and output. In this model R_m is the motional resistor, L_m is the motional inductor, C_m is the motional capacitance. C_0 located in the electrostatic branch is the static feedthrough capacitance of the resonator. The parameters can be calculated from the frequency response of the resonator as shown in Fig.2.5 using Eq.2.14, Eq.2.15, Eq.2.16, and Eq.2.17.

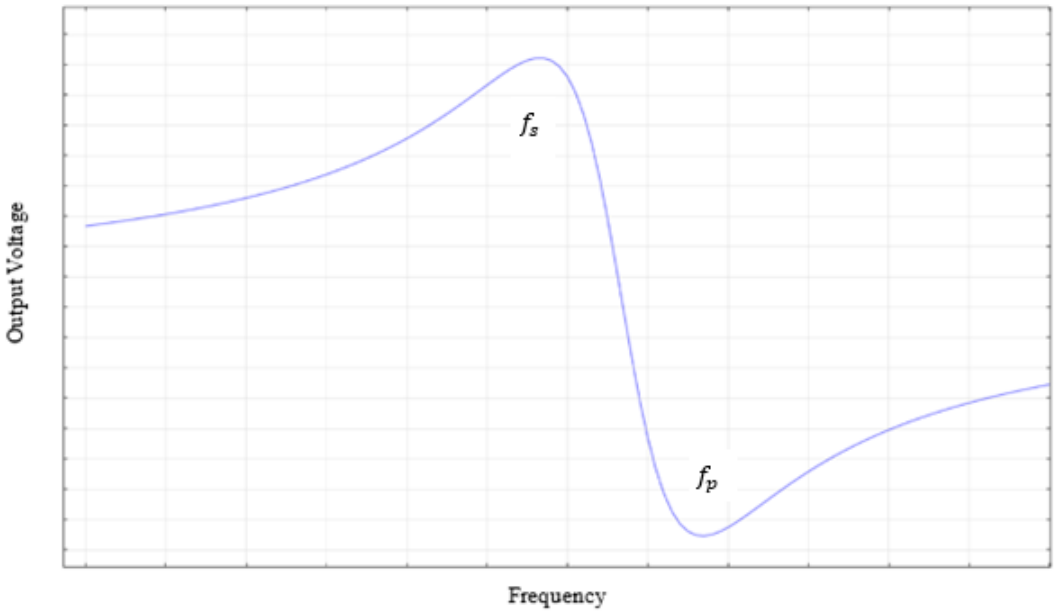

Figure 2.5: Frequency response of a TPOS MEMS resonator.

$$f_s = \sqrt{\frac{1}{L_m C_m}} \tag{2.14}$$

$$f_p = \sqrt{\frac{C_m + C_0}{L_m (C_m C_0)}} \tag{2.15}$$

$$Q = \frac{L_m 2\pi f_p}{R_m} \tag{2.16}$$

$$IL = \log \frac{100}{100 + R_m} \tag{2.17}$$

Fabrication Process

As part of this thesis TPoS resonators with silicon substrate were fabricated. The results The fabrication process consists of 5 masks, as illustrated in Fig.2.6. The process starting with a blank polished single crystalline wafer bonded to a single crystalline handle wafer with an oxide layer in between commonly known as a Silicon On Insulator (SOI). The oxide layer acts as a etch stop. An ultra-thin layer of 5nm of AlN is sputter deposited on top of the wafer. Since AlN is a insulator this thin layer will prevent electrical contact between the silicon substrate and the top layers. Additionally this layer will serve as a seed layer for depositing highly c-axis oriented AlN in the following steps. Following this, a layer of Molybdenum is sputter deposited. This layer will serve as the ground electrode. To define the shapes of the ground electrodes a photoresist mask is used to etch Molybdenum in O_2 and SF_6 plasma Fig.2.6(a).

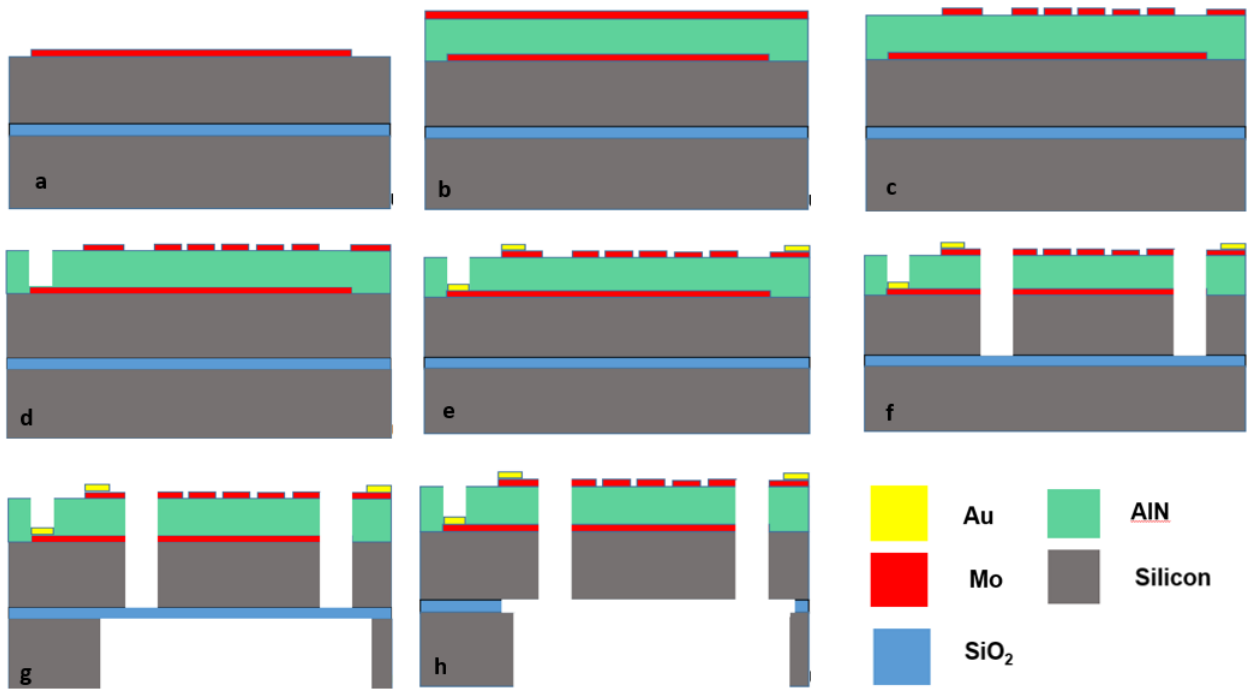

Figure 2.6: Process flow for fabrication of silicon substrate piezoelectric MEMS resonator [2].

The main AlN film is deposited next using a sputtering system. The underlying Molybdenum promotes the growth of c-axis oriented AlN. This is one of the reason Molybdenum was chosen for the electrode. The coupling coefficient of the AlN is determined at this step, therefore this deposition step need to be especially carefully controlled. In the next step a 100nm of Molybdenum is deposited on top of the AlN. This layer forms the top electrode Fig.2.6(b). The previous steps were outsourced with the exception of patterning and etching bottom Molybdenum layer. The following steps were performed at various cleanrooms at the University of Central Florida.

To create access to the ground electrodes the top Molybdenum layer is etched in O_2 and SF_6 plasma using an oxide and photoresist mask Fig.2.6(c). After the top Molybdenum is etched the underlying

AlN is etched in heated RD6 solution. RD6 contains Tetramethylammonium Hydroxide (TMAH) which reacts strongly with AlN, removing the layer and exposing the underlying Molybdenum Fig.2.7(d). The end result is shown in Fig.2.6(d). Molybdenum oxidizes in atmospheric oxygen, therefore a 80nm Gold layer with a 10nm Germanium adhesion promotion layer was deposited with an e-beam system Fig.2.6(e). Lift-off was utilized to create the desired patterns.

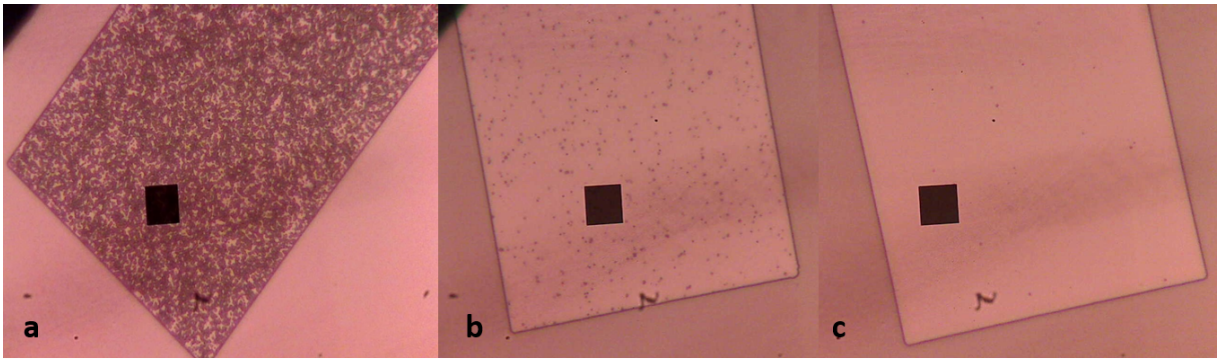

Figure 2.7: Top view of ALN etched in RD6 heated to 90°C for (a) 30s, (b) 270s (c) 395s. The dark squares are a feature of the optical microscope.

At this point all layers of the MEMS device have been deposited, and the following steps involves defining the geometry of the MEMS device by selectively etching the microstructures' boundaries. An oxide mask is deposited on the top side of the wafer and also on the backside of the wafer. Using this oxide mask the stack of top Molybdenum, AlN, and bottom Molybdenum are etched in Chlorine plasma. The substrate silicon layer is etched with a Deep Reactive Ion Etching (DRIE) system using the Bosch system to have straight sidewalls perpendicular to the to the wafer's surface.

At this stage the MEMS device is only attached to oxide underneath it and has been released from all other sides Fig.2.6(f). To remove the oxide located between the two silicon layers the

wafer etched from the back side using the DRIE system Fig.2.6(g). The etch continues until the handle wafer is etched through and the oxide layer is exposed. In the final step the wafer is placed in Hydrofluoric Acid (HF) which etches away the oxide and completes the release of the device Fig.2.6(h). Fully fabricated and released devices are imaged using SEM and shown in Fig.2.8 and Fig.2.9.

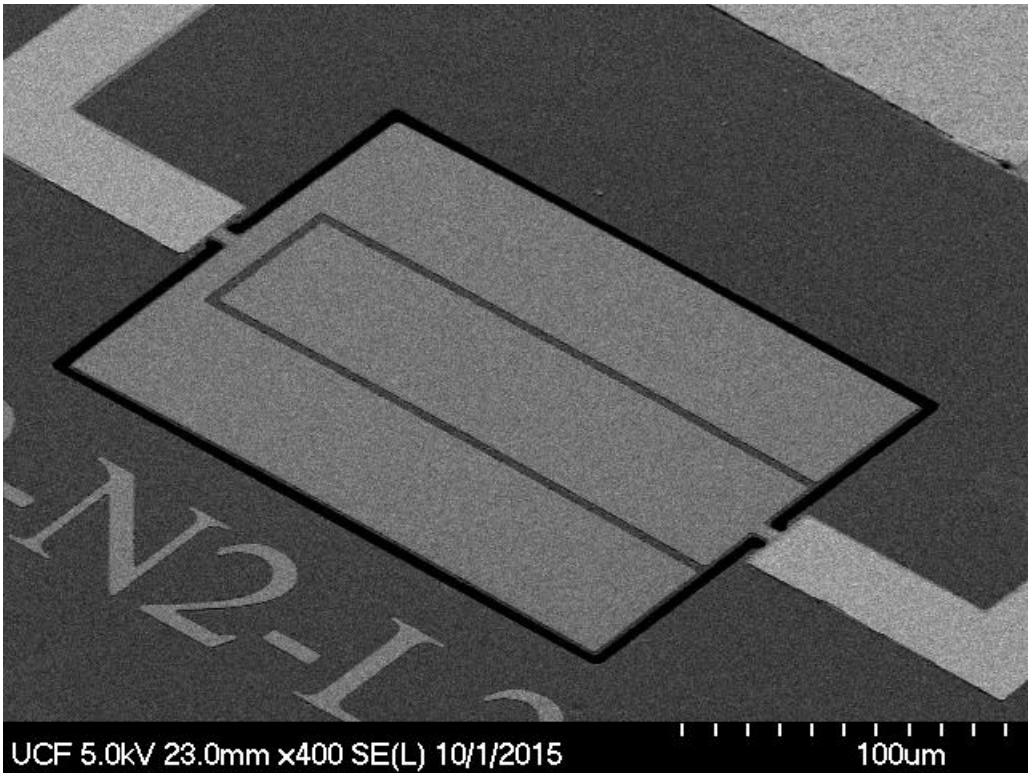

Figure 2.8: SEM image of silicon substrate TPoS MEMS resonator

TPoS resonators with silicon substrate were found to be inadequate for our purposes. Instead, diamond substrate TPoS devices which were not fabricated were as part of this work but were already available were utilized. Readers are encouraged to study the fabrication process of diamond substrate TPoS devices in [2].

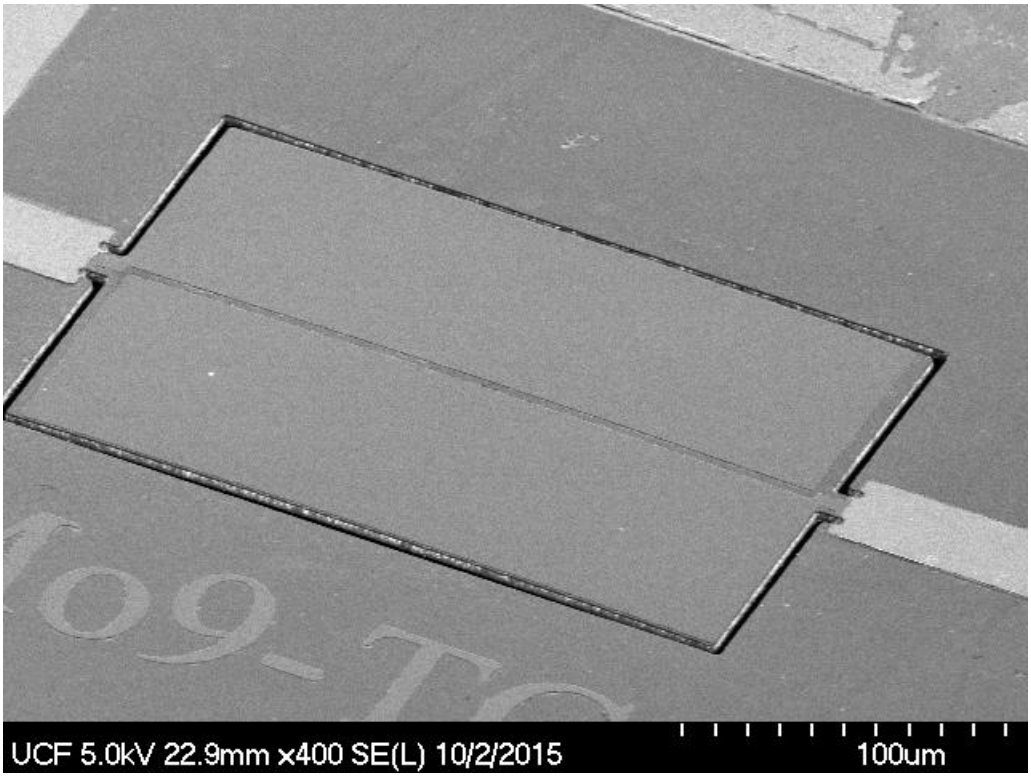

Figure 2.9: SEM image of silicon substrate TPoS MEMS resonator

CHAPTER 3: RESPIRATION MONITORING

Wireless Sensing Overview

The sensor developed in this study is passive and therefore requires an external power source to function. To this end an external antenna transmits an excitation signal. As the sensor is energized it transmits a response signal. The response signal is received by an external receiver antenna. Given that the power of the response signal is much weaker than the excitation signal, the excitation is pulsed as depicted by Fig.3.1. In every pulse cycle the receiver antenna receives a response from the sensor which it analyzes using a Fast Fourier Transform (FFT) algorithm. The data received from the sensor in each pulse cycle is converted to a single data point. Effectively, the higher the frequency of the pulse, the higher number of data points per unit of time, the more detailed the profile. The respiration is plotted by plotting these data points against time.

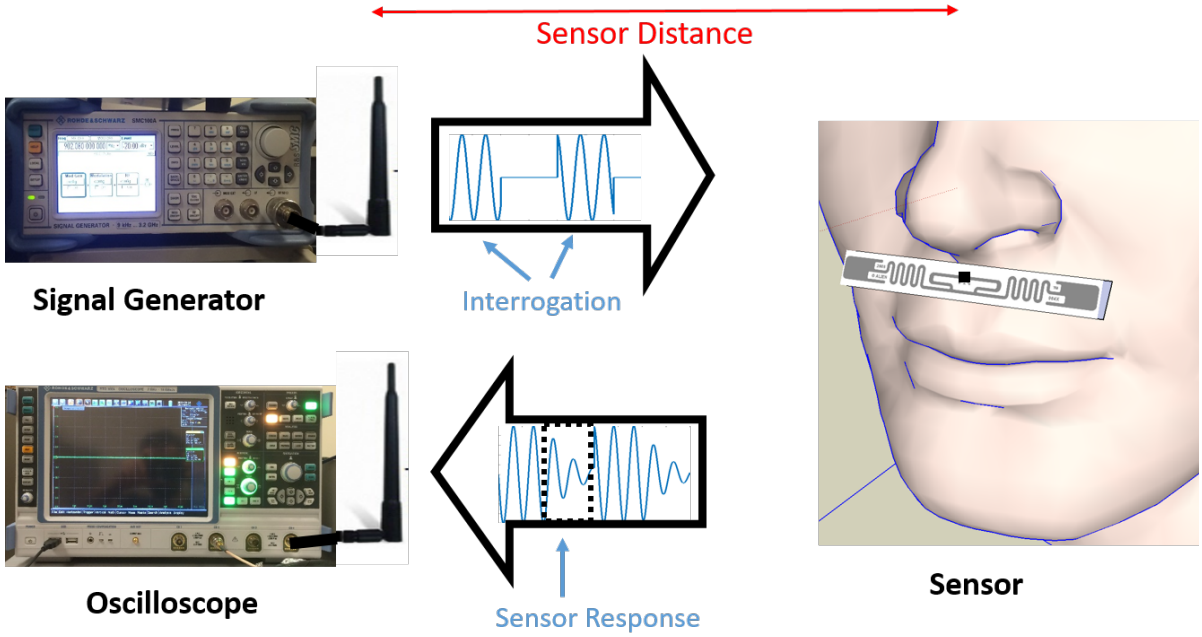

Figure 3.1: Measurement system used for monitoring the respiration profile

The response from the sensor is in the form of an exponentially decaying sinusoidal. The effective duration of the response is the time between when the amplitude of the excitation signal drops to zero and the point where the amplitude of the response signal drops below the noise floor.

One of the main limiting factors of our sensor is the low power response from the sensor. This significant loss in power is not limited to our sensor but is a characteristic of passive wireless sensor measurement . Several approaches have been developed for overcoming this obstacle. Low signal power means that the measurement is susceptible inaccuracy caused by noise. By applying narrow passband filters -both digital and physical- it's possible to reduce the effect of noise on the signal and hence improve accuracy.

This method has the drawback of adding a level of complexity to the measurement setup, increased

hardware cost in the case of physical filters, and longer processing time in the case of digital filters. Increasing the power of the excitation signal will result in an increase in the power of the response signal from the sensor. An increase in the power of the response signal means that it's much less susceptible to noise, especially noise from the antennae, the channel, and the resonator. This approach however has significant draw backs. Amplifying a high power signal such as the excitation signal requires a low noise, high power, high gain amplifier. Due to the stringent requirements such amplifier are costly. Furthermore, such amplifiers use significant amounts of power and produce a considerable amount of heat, both highly undesirable outcomes. More importantly, high power RF EM waves are generally detrimental to human health. The FCC and FDA have both capped the power of transmitter antennas of mobile phones.

By placing an amplifier at the receiving end it's possible to circumvent the problems arising from high EM RF power. Since the signal at the receiver end has undergone the biggest source of power loss there is no need to for high power amplification but rather high gain amplification is desired. The major drawback of this method in addition to the cost of low noise low power amplifier is that this amplifier can reduce the effect of noise in the subsequent sections of the measurement system (i.e. AD converter, etc.) it is unable in canceling the noise stemming from the antennae, channel, and resonator. It has a added bonus of eliminating the need for low voltage AD converter which can be expensive. Finally, the effect of noise can be reduced by using effective signal processing methods. Averaging is the most well-known noise reduction method based on signal processing. By taking the average of sensor's response from several consecutive cycles it's possible to reduce the effect of noise in the measurement. The downside is that in addition to an increase in the processing time by using this method effectively several data points are combined to create a single data point. Since the average respiration cycle is approximately 4 seconds and the profile is required to follow this respiration very closely there is a strict upper limit for the number of measurement cycles that can be averagedbefore the number of data points are inadequate to

faithfully reproduce the profile. Low power Analog-to-Digital converters can help to reduce the noise of the input signal by improving detection sensitivity.

Sensor Distance

Calculation of the maximum permissible distance between the sensor and the external transceiver is directly dependent on the Signal to Noise Ratio (SNR). Since freedom of movement is the key feature of the sensor, improving the maximum sensor distance is essential. This distance has been highlighted in Fig.3.1. The steps explained in the previous section for noise reduction help to increase the sensor distance. It's possible to calculate an estimate of the power of the received signal from the sensor using Friis equation [13] (Eq.3.1).

$$\frac{P_r}{P_t} = G_t G_r \left(\frac{\lambda}{4\pi R}\right)^2 \tag{3.1}$$

Where P_r is the received power, P_r is the transmitted power, G_t is the gain of the transmitter, G_r is the gain of the receiver, λ is the wavelength, and R is the distance between the sensor and the antennae.

Readers are cautioned in using this equation since it ignores loss in the sensor, the contribution of noise and assumes omni-directional antennae. Despite this, Eq.3.1 is effective in providing a rough approximation of the sensor response.

Data Acquisition

Fast Fourier Transform (FFT) algorithms, similar to Fourier transform, mapsa signal from the time domain to the frequency domain. The major advantage of FFT over other Fourier transforms is its efficiency. This has the resulted in widespread utilization of FFT algorithms in not only in communication systems but throughout all fields and applications.

The resonance frequency of the sensor changed as a function of temperature and moisture condensation. The response of the sensor to the excitation signalis in the form of a decaying exponential function with its amplitude modulated with a sinusoidal. When mapped to the frequency domain the resonance frequency can be identified as the highest peak in the spectrum. In order to faithfully produce the frequency spectrum a signal using FFT analysis a minimum number of data points in the time domain is required. This minimum number is determined by the maximum frequency that we would like to analyze. For example to analyze a signal with a frequency of 3.1GHz a minimum sampling rate of 6.2GHz is required.In cases such as this example, where the minimum sampling rate is significantly large, typical measurement systems may be insufficient. To circumvent this problem it's possible to reduce the frequency of the signal without distorting it by multiplying it with an external sinusoidal signal.Using this technique for previous example the sampling rate can be reduced to 0.2GHz if the original signal is multiplied by a sinus wave with a frequency of 3GHz. This technique is widely used in communication industry including all mobile phones and has been highly developed and optimized. The drawback of this method is that it requires a additional equipment such as a low pass filter, adding to the cost and complexity of the measurement system.

After the receiving antenna receives the sensor's response signal (it is passed through a low-noise low-power high-gain amplifier and a low pass filter) the signal reaches the AD converter. This marks the end of the analog section of the measurement system. This data is sent via an ether-

net cable to the processing unit which operates LabVIEW. The measurement system is shown in Fig.3.1.

The measurement system operates by extracting the resonance frequency of the sensor from its response signal. Respiration causes a shift in the resonance frequency of the sensor. In order to produce an accurate profile the measurement system must be capable of faithfully reproducing the resonance frequency of the sensor from FFT analysis of the response signal. However, FFT is a discrete transform meaning that the frequency spectrum does not exist in all frequencies, rather it exists in discrete steps. This is an inherent limitation on the accuracy of the measurement system. To shorten the frequency step size we must increase the acquisition time in each response measurement. Increasing the acquisition time itself is in turn limited by the noise floor. When the power of the signal drops below the noise floor the signal is effectively undetectable. It is possible to improve these constraints by reducing the noise level or increasing the signal amplitude with an amplifier, however since each additional stage is accompanied by costs and complications at a certain level the benefits are outweighed by the costs and defeat the purpose of this sensor which is to provide an inexpensive alternative to the current technology.

Sources of Power Loss

Of the power accessible to the sensor only a portion of it is utilized and the remainder is converted to heat. Of the EM waves incident on the sensor's antenna (RFID), a portion is reflected off into space. Similarly only a portion of the power received by the RFID is transferred to the resonator. The maximum power which can be transferred to the resonator is only 50% of the EM power converted by the RFID antenna, a further inherent limitation to the measurement system. The response of the resonator is subject to a similar loss mechanism.

Parameters Used in Respiration Monitoring

With each respiration cycle a number of the human body's biological parameters fluctuate according to the respiration cycle . Based on these parameters various sensing systems have been devised. In this section we will review the parameters used by sensors for respiration monitoring.

1- Flow: The process of drawing fresh air into the lungs and pushing out the exhaust is accompanied by periodic changes in air flow. Air flow is defined as either the net volume or net mass of air passing through a closed loop in a unit of time. The number of molecules, their mass, and velocity all impact the air flow. For this reason, measurements of air flow sensors need to be carefully normalized according to the patient's age, gender, etc. As an example, compared to a child an adult has a much larger respiration system, therefore, the number of air molecules entering the lungs per cycle is larger.

2- Pressure: The pumping mechanism used in the human respiration process is based on creation of positive and negative pressure in the lungs. Lungs are made of flexible tissue and is therefore capable of change in its volume. At the beginning of inspiration stage in the respiration cycle, the lungs are at their minimum volume; a result of expiration in the previous cycle. The lungs then expand, decreasing the pressure. The negative pressure causes a rush of air from outside the body into the respiration system. As the air starts to flow into the lungs the pressure steadily increases and the rate of gas (O_2, CO_2, H_2O) exchange increases and finally the lungs reach their maximum volume. At this stage CO_2 and H_2O partial volume is at peak value. This marks the end of the inspiration stage and the lungs begins to contract.

The decreased lung volume results in an increase in pressure in the lungs and flow of air out of the lungs. This cyclical change in pressure can be easily detected using a pressure sensor. Pressure sensors typically operate by measuring the force applied to a section of the sensor with a known

area. The pressure of a gas is a function of temperature, chemical composition of the gas and the number of atoms or molecules of each chemical

3- Temperature: As part of the human body the respiration track maintains a temperature of 37.8C. Heat exchange will reduce the difference in temperature between air passing through the respiratory track and the respiration track itself. Since the heat capacity of the respiration track tissue is much more than that of air, its change in temperature is much smaller.

Air pumped out of the lungs during expiration has a markedly different temperature than the air pumped into the lungs during inspiration. Measuring this temperature difference is one of the most accurate methods for respiration monitoring and is considered as the gold standard of respiration sensing [10].

4- Movement : Respiration is accompanied by movement of the chest area with the increase and decrease of lung volume. This movement can be detected either by analyzing the acoustic or electromagnetic waves reflecting off or coming from the body. Similarly a sensor can be placed directly in contact with the chest and the movement can recorded. A number of piezoelectric sensor have been developed for the latter case [14]. Typically the patient straps a belt around the chest, as the volume of the lungs increases the belt is strained. This mechanical strain is converted to an electrical signal by a sensor.

5- Blood Oxygenation (or CO_2): All human cells require oxygen as a source of energy and produce CO_2 as a byproduct. During inspiration fresh air is driven into the lungs, and O_2 from the air is exchanged for H_2O and CO_2 from the blood. This results in the increase of the blood's O_2 content and decrease of its CO_2 content. Conversely, during expiration as the body is pushing air out of the lungs little gas exchange occurs, cells consume O_2 and create CO_2, increasing the bloods CO_2 content while diminishing its O_2 content. The accumulation of CO_2 and reduction of O_2 is used as a parameter for sensing respiration. This sensing mechanism often requires access to the blood.

6- Chemical sensing: The increased partial volume of CO_2 in the exhaled air as compared to the inhaled air can be sensed with a chemical sensor [9]. Similarly O_2 and H_2O content differ in the exhaled and inhaled gases. By measuring the relative content of gases repeatedly it's possible to monitor the respiration.

7- Acoustic: Respiration process creates acoustic waves of different frequencies, many of which can be easily detected by the human ear. By using a relatively sensitive microphone and a filtering out interference from the environment it's possible to measure the respiration rate [9].

Effect of Respiration on MEMS Resonator

There are three possible avenues of interaction between the MEMS resonator and respiration.

1) Air flow (air pressure): Inspiration and expiration are accompanied by the flow of air molecules to and from the mouth and noise. The mass movement of molecules in a cohesive direction results in the exertion of a net force to any surface in the flow path. This is the operational mechanism of many flow sensors.

2) Temperature: During inspiration air from the environment is drawn towards the lungs. In the lungs a portion of O_2 molecules are exchanged with CO_2 and H_2O molecules. Since these H_2O and CO_2 molecules are extracted from the body their temperature is higher than other molecules. Furthermore, as air is passing to the lungs and while it's in the lungs air molecules are constantly interacting with their environment. This interaction results in an increase in their temperature. In the expiration step air is pumped is out of the lungs. These air molecules hit objects in their flow path. During this interaction part of the thermal energy gained in the lungs is lost to incident surfaces.

The elastic properties of the MEMS resonator's constituting material have a strong impact on its resonance frequency. The elastic properties of material change as a function of temperature. An intuitive model is to assume the resonator as an oscillating mass attached to a spring. If the stiffness of the spring changes with temperature the oscillation will also change.

The stiffness of the constituting materials of our MEMS resonators change linearly with temperature in the range of temperatures studied here. This makes it an excellent candidate as a temperature sensor.

3) Condensation: H_2O molecules condense on cool surfaces. This phenomenon is known as dew and occurs naturally. When the temperature drops below the dew point water molecules condense to create droplets. This occurs more readily on cool surfaces. The surface of the MEMS resonator is exposed to the air flowing to and from the respiration system. Because of high H_2O vapor pressure of expiration this especially prominent. The rate at which the condensed water vapor evaporates is fast enough to not be an impediment to respiration monitoring. In the intermediate time the condensed water acts as a mass load on the resonators surface and increases acoustic scattering on the surface. While the latter's effect is mainly an increase in power loss, the former, in addition to increasing the power loss it results in a substantial shift in resonance frequency. This shift is linearly proportional to the temperature. Assuming that the temperature of the respiration track is constant a deeper breath will cause a larger shift in frequency as more water molecules condense on the surface of the MEMS resonator. The shift in frequency is the parameter of interest in our measurement system.

Change in loss can also be used as a measurement parameter. In this case the amplitude of the response signal is modulated by respiration. In wireless measurement where noise is major limiting factor using loss as the measurement parameter is at a significant disadvantage.

Challenges in Respiration Monitoring

Traditional respiration monitoring systems impose a large constraint on the patient's mobility. Parts of the measurement system in contact with the patient -either directly or indirectly through air flow- need to be replaced whenever possible. However, costs of several sections of the measurement system is such that replacing them for each patient is not financially feasible. This includes the sensing unit and in some devices the mask and tube connected to the patient. Such sections of the measurement system need to be sanitized where possible. Even in the case of well-designed systems where the operator has easy access to all sections of the measurement system the need for constant sensitization increases the chance for human error and creates risk of transmission of illness from patient to patient.

This issue is addressed in our sensor, where the sensor has been designed to be cheap enough to be considered disposable and therefore completely eliminate the chances of transmission of any illness.

CHAPTER 4: RESULTS AND DISCUSSION

In this chapter the results of implementing a measurement system according to the framework discussed in the previous chapters are discussed. A TPoS resonator with a nanocrystalline diamond substrate was utilized as the respiration sensitive component of the sensor. A Molybdenum/AlN/Molybdenum stack was utilized to actuate the resonator. Details of the fabrication process can be found in [2]. The nanocrystalline diamond resonators used here were already fabricated and accessible and were not fabricated as part of this thesis. The device was wirebonded to a commercial ALIEN 9640 RFID tag using aluminum wirebonding threads. Fig.4.1 shows the top view of the resonator taken by an optical microscope. The wirebond pads are also visible. An overview of the RFID antenna along with a wirebonded TPoS resonator is shown in Fig. 4.2

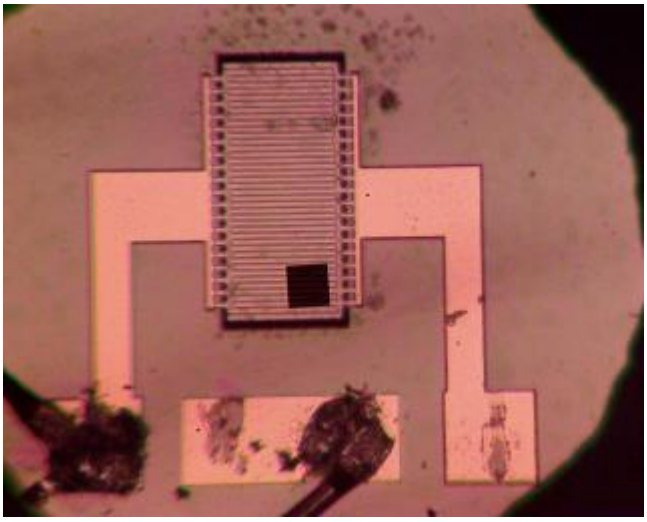

Figure 4.1: High frequency resonator from the top view pictured using optical microscope. The wirebonds attached to electrodes are visible in the lower half. A single input and the ground electrode have been wirebonded. The dark square is a feature of the microscope.

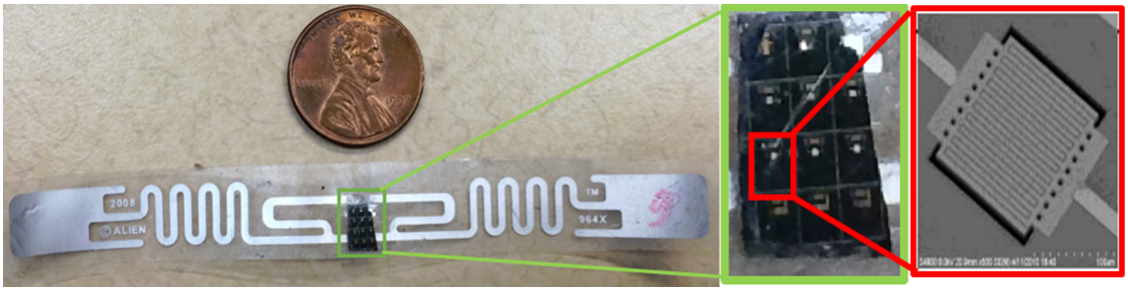

Figure 4.2: Overview of the sensor, from left to right: respiration sensor, wafer piece containing several devices with the wires of the wirebond visibly attached to the device, SEM image of a nanocrystalline diamond resonator [4].

The reason nanocrystalline diamond devices were chosen was because of the very low acoustic loss of nanocrystalline diamond. This results in a low insertion loss at high frequencies [2]. The resonance frequency of the device used in the experiments was 901.8MHz. This device is connected to a flexible antenna. To maximize the absorption of incoming EM waves the resonance frequency of the resonator and the RFID antenna need to be very close. To illustrate the importance of matching the resonance frequency of the resonator and that of the antenna the reflection (S11) of a resonator attached to a flexible antenna was measured for a range of frequencies and is shown in Fig.4.3. A significant disparity between the two frequencies will hinder efficient energy transfer between the antenna and resonator and vice versa.

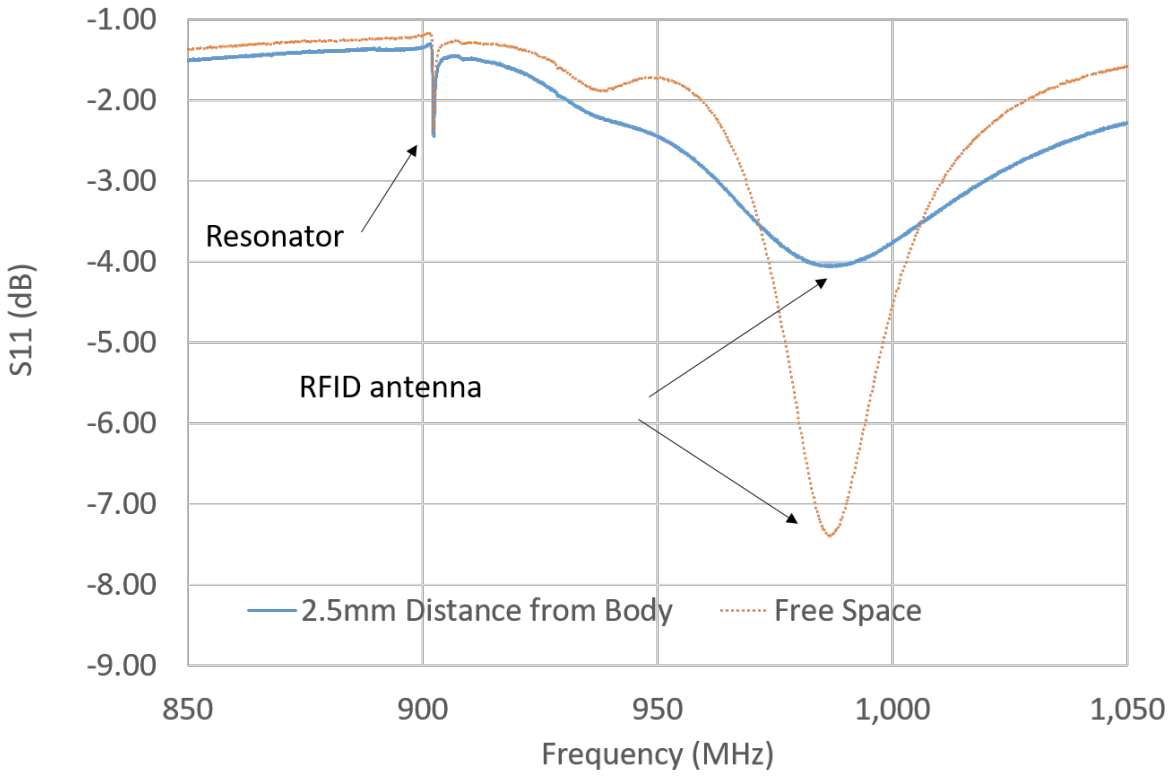

Figure 4.3: Frequency response of a TPoS resonator attached to a flexible antenna.

The mismatch between the resonator, the antenna, and wirebond thread need to minimized. For this end the resonator and antenna's equivalent circuits were derived. The resonator's equivalent circuit, modeled using the Butterworth-Van Dyke (BVD) method is shown in Fig.2.4. To verify the accuracy of the modeled circuit, the equivalent impedance of the resonator was compared to that of the measured impedance in Fig.4.5. The measurement was performed using a Rhode & Schwarz ZNB 8 vector network analyzer.

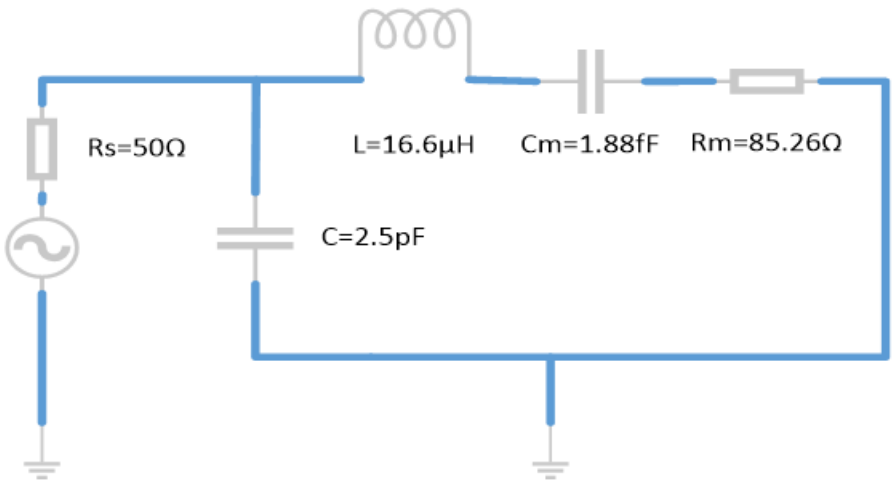

Figure 4.4: BVD model equivalent circuit of 901.8MHz resonator.

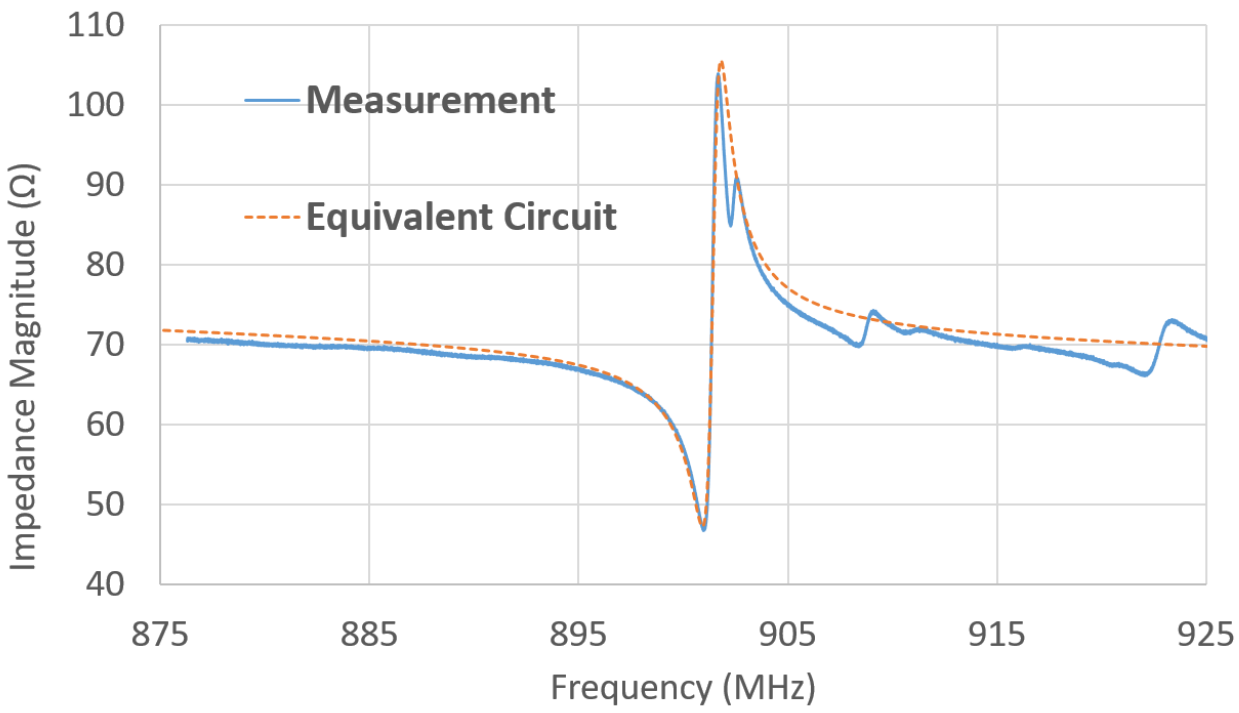

Figure 4.5: Sensor response and response of BVD model equivalent circuit.

As explained in the previous chapter, a signal generator (Rhode & Schwarz SMC100A) generates a pulsed sinusoidal signal. To increase the sensor distance an amplifier (ZFL-2500VHX+) with a gain of 20dB is placed between the signal generator and transmitter antenna. On the receiver end, the response of the sensor is received by a RF antenna and then passes through a 40dB amplifier (MPA-10-40). This amplifier is placed between the receiver antenna and oscilloscope (Rhode & Schwarz RTO 1024). The oscilloscope contains the Analog-to-Digital converter and after converting the analog signal sends the received data to the processing unit which utilizes FFT analysis to extract the sensor's resonance frequency for a single measurement cycle (Fig.4.2). The respiration

profile is calculated by plotting these data points againt time. The measurement system is shown in Fig.4.6 and the sensor is shown in Fig.4.2. The respiration profile was measured for a sensor to transmitter-receiver antennae distance of 25cm.

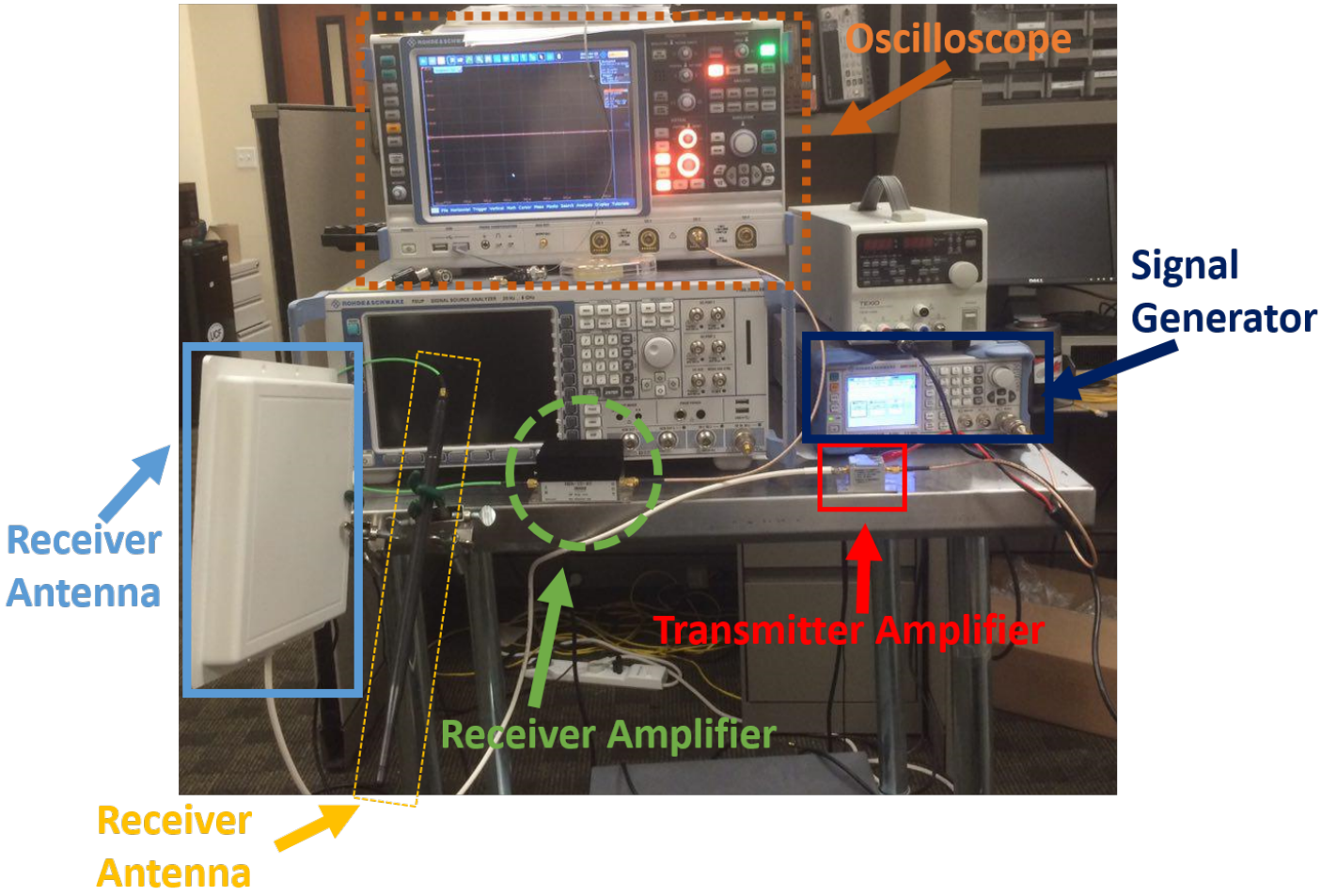

Figure 4.6: Measurement setup used in this study. Sensor is not shown in this figure.

The output signal at the receiving antenna for one measurement cycle is shown in Fig.4.8. The interrogation signal and the response of the sensor can be clearly differentiated.

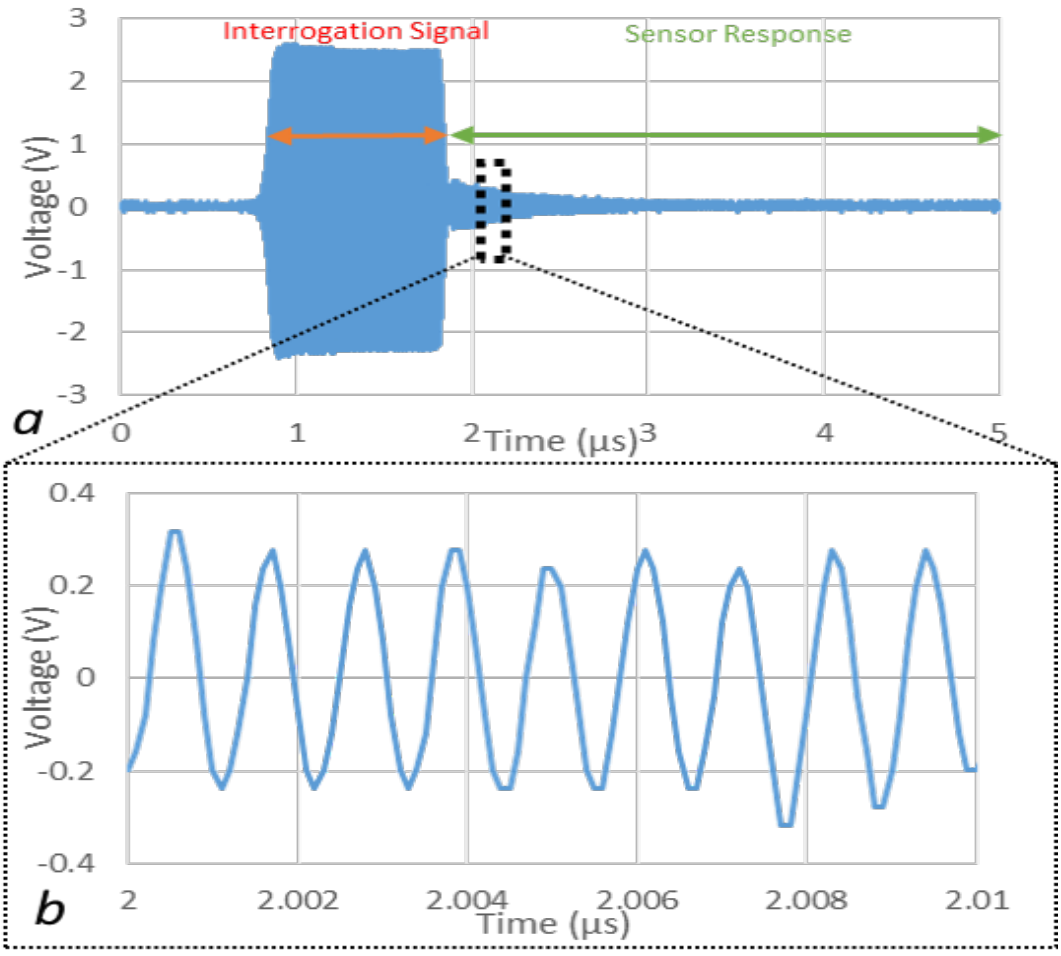

Figure 4.7: time domain response of sensor.

The nasal flow of a healthy adult subject was measured for 200s with this sensor and the results are shown in in Fig.4.8. The distance of the sensor to the receiving antenna was approximately 25cm. The respiration profile for 7 cycles has been shown in detail by Fig.4.8(b). Each data point shown by an orange dot represents an entire measurement cycle as shown Fig.4.7. The average length of each respiration cycle was measured to be 5s. The flow rate of the sensor has not been quantified yet therefore the y axis in Fig.4.8 does not have a unit, nevertheless the overall profile

and respiration can be accurately derived from this figure.

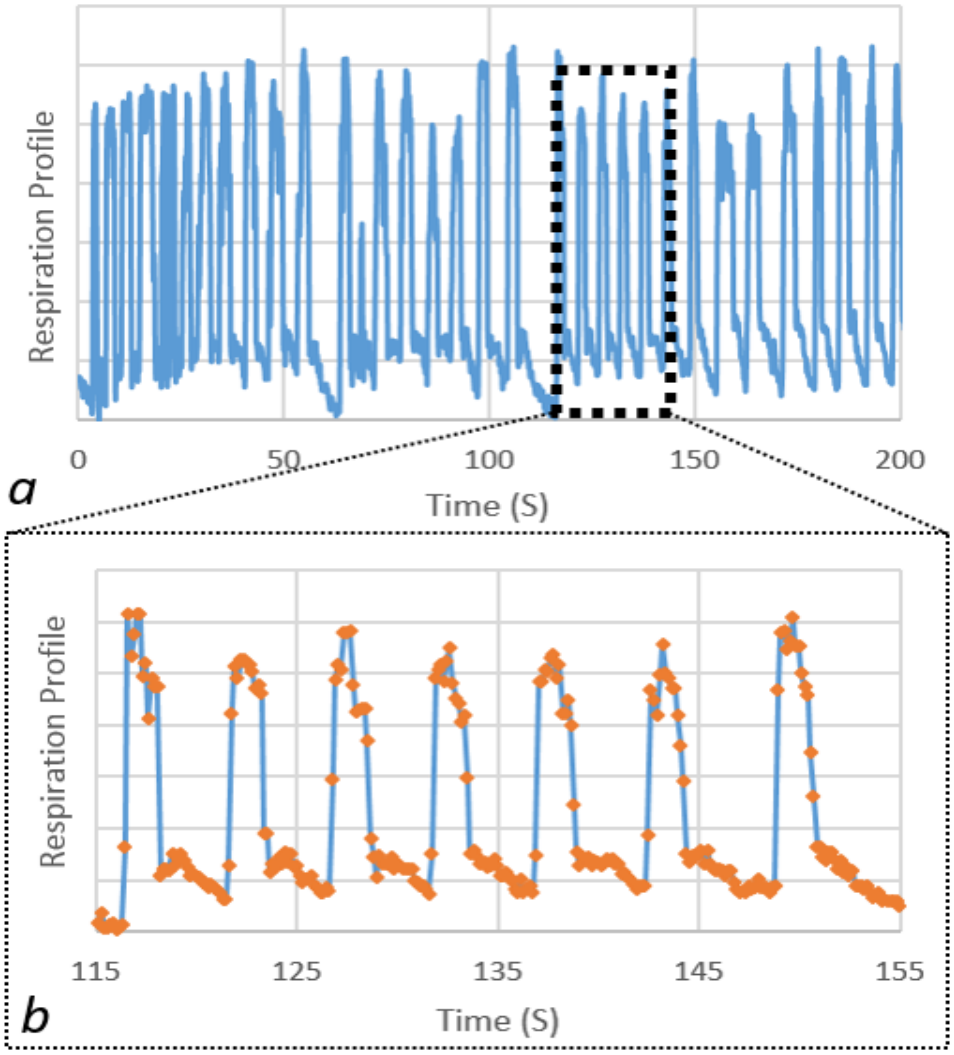

Figure 4.8: Measured respiration profile.

Currently the time resolution of the measured data is approximately 0.2s which is limited by the rate of data transfer from the oscilloscope -which is connected to the receiver antenna- to the computer processing unit that is used to perform FFT analysis on the measured data points. The current

data transfer rate value is sufficient for recording the the respiration rate, the peak value for each cycle, and to faithfully follow the overall profile. However, the time resolution of the measurement could be considerably improved by developing a dedicated processing unit with enhanced processing power and increased data transfer rate. Improvement of resolution will enhance the sensor's sensitivity towards small details of the respiration process, thus making it capable of detecting slight variations in the respiratory system. Also, an increased number of data points and processing power can be used to reduce the SNR by performing averaging with increased number of recorded samples.

Effect of Moisture and Temperature

As shown in Fig.3.1 the sensor is placed above the upper lip and is in contact to inhalation and exhalation flow. As a result the sensor is exposed to both changes in flow temperature and moisture. Change in the sensor's resonance frequency is a function of both of these parameters. To understand the effect of each these parameters a sensor was exposed to airflow heated with an electric heater and subsequently exposed to respiration. The results of this experiment are shown in Fig.4.9. These results show that the condensation and evaporation of moisture in each respiration cycle has a more significant effect on the shift in resonance frequency of the sensor and that the current sensor is not capable of measuring the respiration profile solely based on the cyclical change in respiration flow temperature.

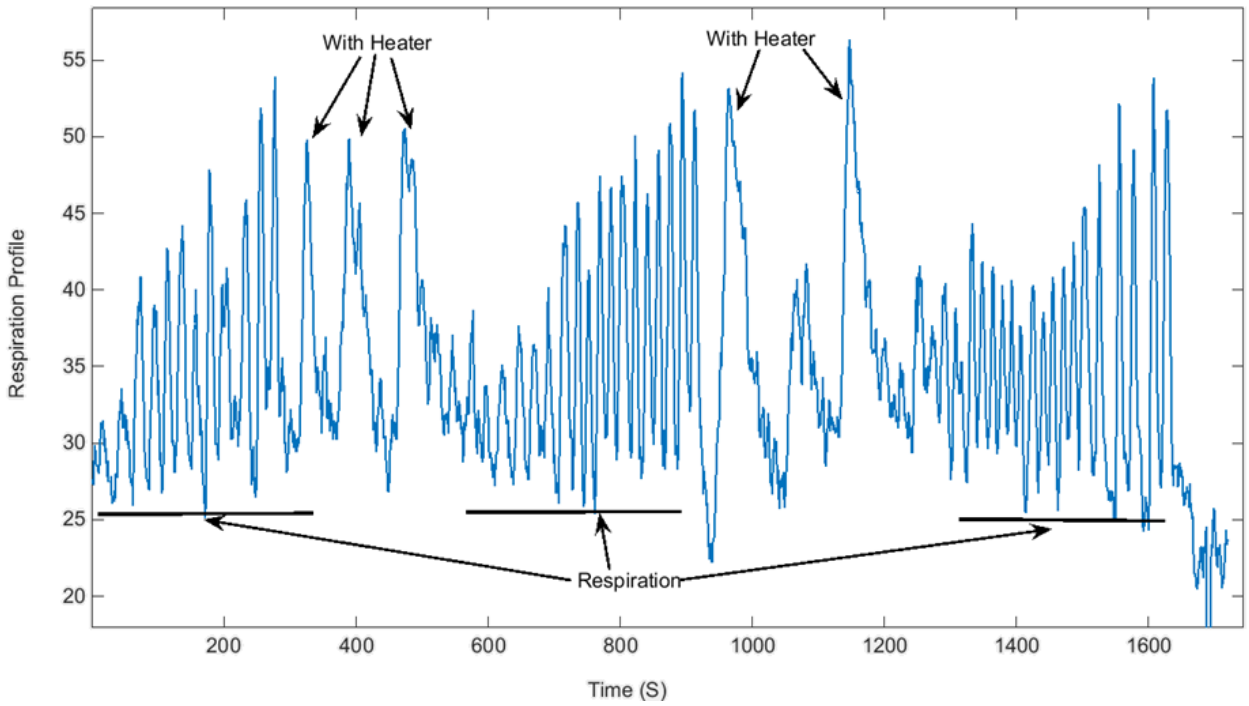

Figure 4.9: Comparison of the effect of moisture condensation and temperature change on the performance of the respiration sensor.

Verification of Sensor

To further verify the respiration profile measured by this sensor its result was compared to that measured by a thermocouple. Measuring the respiration rate with a temperature sensor such as a thermocouple is currently the gold standard of respiratory monitoring [10]. A k-type thermocouple is placed very close to the nasal track. The periodic change in temperature is converted to a periodic voltage. This voltage is plotted against time and compared to the respiration profile measured by

our sensor in Fig.4.10. The two profiles clearly closely resemble one another, confirming the operation of the respiration sensor studied in this thesis.

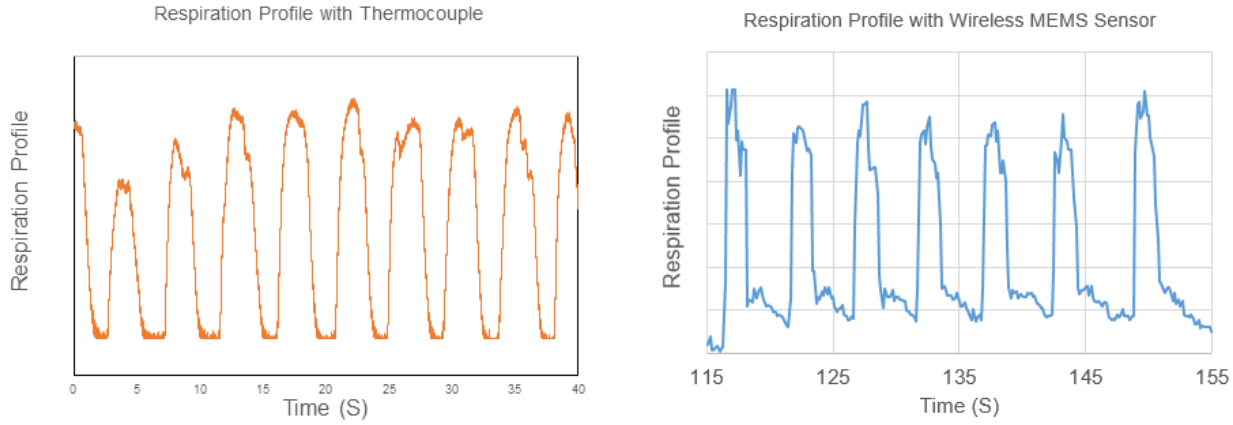

Figure 4.10: Comparison of respiration profile measured using the gold standard (left) to that of wireless passive MEMS sensor (right).

CHAPTER 5: CONCLUSIONS AND FUTURE WORK

Conclusion

A respiration sensor has been developed with the main goal of providing an inexpensive, easy to use, lightweight, and robust alternative to the current available technology. The sensor is composed of a TPoS MEMS resonator attached to a flexible UHF RFID antenna. The sensor is excited via an external transmitter and its response is analyzed via FFT. The resonance frequency is derived from FFT analysis and used to plot the respiration profile. Respiration results in a periodic change in the temperature of the resonator. Additionally increased moisture content in expiration results in the dampening of the acoustic waves and a decrease in resonance frequency.

The deposition water vapor onto the surface. Both increase in temperature and condensation of moisture result in a decrease in resonance frequency. The sensor was found to be operational from a distance of 25cm and was capable of following the respiration profile measured using a thermocouple which is the gold standard.

To reduce the effect of noise on the signal and improve the accuracy and also increase the sensing range two amplification stages as well signal processing were implemented.

Future Work

To improve the respiration sensing system both the measurement system and the sensor itself need to be modified. The following improvements are recommended:

1- The exposure of the surface of the resonator to expiration while increasing the sensitivity of the

sensor, in the long term increases the likelihood of irreversible damage to the resonator. Therefore the resonator needs to be packaged using a material with high thermal conductivity and low heat capacity.

2- To maximize the change of resonance frequency as a result of temperature change several approaches are recommended:

A- The TCE of the resonator's constituting material must be increased. This can be accomplished by increasing doping levelsor using different materials altogether.

B- Optimization of the design of the resonator by modifying parameters such as microstructure geometry and thickness of layers with the objective of maximizing TCF and electrical performance at the same time.

C- Using a dedicated processing unit instead of a PC increases the recorded data points and allows implementation of noise reduction methods such as averaging.

D- Placement of multiple receiving antennae in various locations to improve both the patient's mobility and decrease the noise level by having multiple measurement points with different paths.

E- Decrease the gain of the amplifier at the transmitter and compensate with increasing the gain of the amplifier at the receiver end. This reduces the patient's exposure to high power RF EM waves however it also decreases accuracy which.

LIST OF REFERENCES

[1] Wikipedia, "Polarisation (elektrizitt) — wikipedia, die freie enzyklopdie," 2015. [Online; Stand 25. Mrz 2017].

[2] H. Fatemi and R. Abdolvand, "Low-loss lateral-extensional piezoelectric filters on ultra-nanocrystalline diamond," *IEEE transactions on ultrasonics, ferroelectrics, and frequency control*, vol. 60, no. 9, pp. 1978–1988, 2013.

[3] R. Abdolvand, H. Fatemi, and S. Moradian, "Quality factor and coupling in piezoelectric mems resonators," *Piezoelectric MEMS Resonatorsl*, pp. 133–152, 2017.

[4] S. Moradian and R. Abdolvand, "Mems-based passive wireless respiration profile sensor," in *SENSORS, 2016 IEEE*, pp. 1–3, IEEE, 2016.

[5] B. Harrington, M. Shahmohammadi, and R. Abdolvand, "Toward ultimate performance in ghz mems resonators: Low impedance and high q," pp. 707–710, 2010.

[6] D. Simel, "Approach to the patient: history and physical examination," *Goldmans Cecil Medicine*, vol. 6, 2011.

[7] M. A. Cretikos, R. Bellomo, K. Hillman, J. Chen, S. Finfer, and A. Flabouris, "Respiratory rate: the neglected vital sign," *Medical Journal of Australia*, vol. 188, no. 11, p. 657, 2008.

[8] C. Subbe, R. Davies, E. Williams, P. Rutherford, and L. Gemmell, "Effect of introducing the modified early warning score on clinical outcomes, cardio-pulmonary arrests and intensive care utilisation in acute medical admissions," *Anaesthesia*, vol. 58, no. 8, pp. 797–802, 2003.

[9] F. Q. AL-Khalidi, R. Saatchi, D. Burke, H. Elphick, and S. Tan, "Respiration rate monitoring methods: A review," *Pediatric pulmonology*, vol. 46, no. 6, pp. 523–529, 2011.

[10] B. Mazzanti, C. Lamberti, and J. de Bie, "Validation of an ecg-derived respiration monitoring method," in *Computers in Cardiology, 2003*, pp. 613–616, IEEE, 2003.

[11] F. Irgens, *Continuum mechanics*. Springer Science & Business Media, 2008.

[12] G. G. Raju, *Dielectrics in electric fields*. CRC press, 2013.

[13] C. A. Balanis, *Antenna theory: analysis and design*. John Wiley & Sons, 2016.

[14] K. J. Kim, Y. M. Chang, S. Yoon, and H. J. Kim, "A novel piezoelectric pvdf film-based physiological sensing belt for a complementary respiration and heartbeat monitoring system," *Integrated Ferroelectrics*, vol. 107, no. 1, pp. 53–68, 2009.